Design and Development of a Magnetic-Steered Minimally Invasive Bioprinting System

Haoran Chen, Zichen Xu, Zhengyang Li, *Student Member, IEEE*, and Qingsong Xu, *Senior Member, IEEE*

***Abstract*—Bioprinting is a promising fabrication technique to create medical devices for the human body in vivo or in vitro. However, the existing in-vivo bioprinting methods impose various prerequisites, such as a large incision on the human skin, to make the printing nozzle close to internal organs. Herein, we propose the design of a new magnetic-steered bioprinting system, which can perform bioprinting tasks in a less invasive manner. It is enabled by the introduced concept design of hybrid printing pipe, which integrates the advantages of rigid tube and flexible pipe together. The system consists of two essential parts for direct positioning and printing. After precise positioning, it drives the flexible pipe to deflect under the skin. The printing nozzle is steered by a permanent magnet. Experimental studies have been conducted to demonstrate the printing of both regular and asymmetrical patterns on a pig liver tissue and a flat surface. This work provides a promising solution for printing biological tissues or robots in minimally invasive manner.**

***Index Terms*—3D printing, Bioprinting, flexible tube, magnetic actuation, minimally invasive operation.**

I. Introduction

SINCE its introduction, bioprinting technology has undergone many technological innovations and material changes across multiple fields [1]. It has been applied in various application domains, including medicine, engineering, manufacturing, arts, and education [2], [3]. In particular, bioprinting technology is widely used in medical field [2], [4], [5]. Unlike traditional methods (e.g., scaffolds) to produce precise tissue structures, bioprinting technology's high precision and personalized design allows it to effectively bridge the gap between artificial and native tissues by offering unprecedented versatility [5]. Consequently, it is often adopted to manufacture implants (e.g., skin, bone [4], [6], tissue, and organ [5], [7]).

In addition to the application in medical field, bioprinting technology is also commonly used in biology field [8], [9]. However, compared to its mature use in medical field, there are still technical challenges in biology area, especially in cellular and innervation domain [10]. According to Zhu et al., [11], the traditional 3D printing technology relied heavily on open-loop, calibrated printing procedures before a closed-loop approach (including adaptive 3D printing) was developed to meet the need for manufacturing devices on moving, free-form surfaces. Moreover, 3D printing has also undergone breakthroughs in terms of compactness and precision [12]. At the same time, the technology of 3D printing should progress to meet the needs of application area. For example, the safety risks associated with in-vitro printed tissue cultures and the accompanied complex transplantation processes have stimulated the research on in-vivo bioprinting [13], [14].

In recent years, the bioprinting of personalized and customized designs has gained much attention from researchers [15]. Zhou et al. developed a ferromagnetic soft catheter robot (FSCR) to achieve bioprinting [16]. Because the deflected part of the FSCR is located above the skin, it is easy to cause skin tears during actual printing process. It has been shown that printable functional ink is the key substrate for bioprinting [3], [17], [18], [19]. Relevant work has been conducted to accommodate skin cells and appropriate combinations of cells [20], [21], [22], [23]. By using special materials, 4D printing has been applied to fields ranging from mechanical engineering and materials science to biomedical engineering [24], [25]. Based on 4D printing for biomedical applications, the unique ability to produce dynamic morphological changes in response to specific stimuli enables the printing of micro/nano robots and human organs [26], [27], [28], [29]. Extrusion is the most extensively used accessible bioprinting method. It contains three main methods (Fig. 1(a)). Conventional printing systems use rigid nozzles (Fig. 1(b)), which require cutting a large incision in the skin. Alternatively, flexible tubes can be used as a transportation tool in bioprinting to get direct access to the human body. In this way, the displacement side of the flexible tube is located above the skin. However, the skin will be torn when the transportation tool is moving under the effects of different physical fields (Fig. 1(c)).

To overcome the above issue, we propose a new extrusion bioprinting system by incorporating magnetic actuation with 3D printing techniques in this letter, which is dedicated to minimally invasive in-vivo bioprinting in the human abdominal or thoracic cavity. Different from the conventional methods, we introduce the concept of limit-position pipe, which fuses the merits of rigid and flexible tubes and drives the flexible pipe to move under the skin (Fig. 1(d)). Hence, the human skin needs to be

Manuscript received 23 April 2023; accepted 20 August 2023. Date of publication 4 September 2023; date of current version 11 September 2023. This letter was recommended for publication by Associate Editor J. Liu and Editor X. Liu upon evaluation of the reviewers' comments. This work was supported in part by the National Natural Science Foundation of China under Grant 52175556, in part by the Macao Science and Technology Development Fund under Grants 0004/2022/AKP and 0102/2022/A2, and in part by the University of Macau under Grants MYRG2022-00068-FST and MYRG-CRG2022-00004-FST-ICI. *(Corresponding author: Qingsong Xu.)*

The authors are with the Department of Electromechanical Engineering, Faculty of Science and Technology, University of Macau, Macau 999078, China (e-mail: mc15045@um.edu.mo; yc17914@um.edu.mo; mbxzhengyang@outlook.com; qsxu@umac.mo).

Digital Object Identifier 10.1109/LRA.2023.3311373

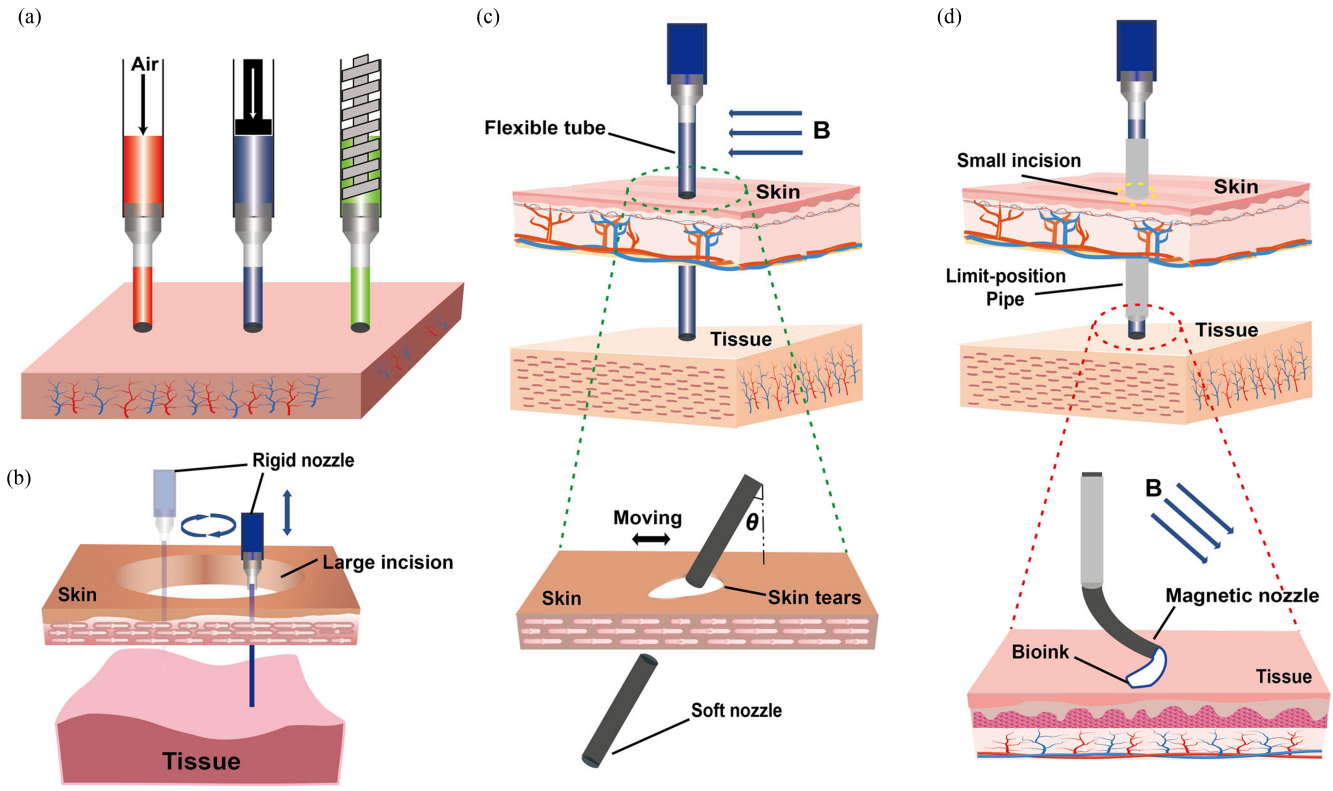

Fig. 1. Schematic of principles for different in vivo extrusion bioprinting methods. (a) Extrusion bio-printing methods: pneumatically driven, mechanically driven under direct piston force, and mechanically driven under screw rotation-enabled force. (b) Traditional printing system using a rigid nozzle with a large incision. (c) In vivo bioprinting based on a conventional flexible pipe and its disadvantage. (d) The proposed minimally invasive bioprinting system.

cut by a small incision, which greatly relieves patients' pain and shortens the recovery time. Experimental results show that the developed bioprinting system can print different patterns using multiple inks.

The remaining parts of the letter are organized as follows. The system design is outlined in Section II. The printing nozzle optimization is carried out in Section III. Experimental results of printing tests are given in Section IV. Finally, Section V concludes this letter.

II. Bioprinting System Design

The proposed bioprinting system works with a printing nozzle steered by a permanent magnet. The system design is outlined in the following.

A. Mechanical Design

The designed minimally invasive bioprinting system is composed of a hybrid printing tube and a magnetic field steering device. The magnetic field steering device consists of four single-axis linear motion stages driven by four stepper motors to realize the motion in space (Fig. 2(a)). In particular, two linear stages are installed in the Y-axis direction to deliver independent up and down movement of two components, i.e., the flexible printing tube and limit-position rigid pipe. The other two stages in the Z-axis and X-axis are stacked together to provide the motion in the XZ plane. A guidance magnet is installed on the XZ platform, which is driven by two linear stages (Fig. 2(b)). The position adjustment of the guidance magnet is achieved by controlling the movement of two stepper motors. The printing platform is made of silicone material in a Petri dish, which is located above the permanent magnet by keeping a certain distance from the guidance magnet.

The hybrid printing tube is constructed by the serial connection of a limit-position rigid tube, a flexible printing tube, and a magnetic nozzle. The rigid tube is made of stainless steel (102Cr17Mo), which is a common material for surgical tools. The flexible printing tube adopts the material of silica gel. In addition, the nozzle material is selected as neodymium magnet (NdFeB) or Ni-Zn ferrite (NiZnFeO), which is installed at the terminal of the tube. The nozzle and flexible printing tube are located above the printing platform. Silica gel is adopted as the printing material, which has passed the bio-compatibility test and will not cause adverse effect after entering into the human tissues. Under the action of a gradient magnetic field, we can control the nozzle to move to any position in the XZ plane by controlling the movement of a steering magnet at the bottom.

B. Control and Guidance Design

The bioprinting system is actuated by four single-axis linear motion stages. Two stages in the XZ plane drive the guidance magnet. The printing tube and nozzle are driven in different up and down directions due to the combined effect of the magnetic field and limit-position pipe. Fig. 2(c) shows the nozzle positions relative to the guidance magnet's upper surface. For illustration,

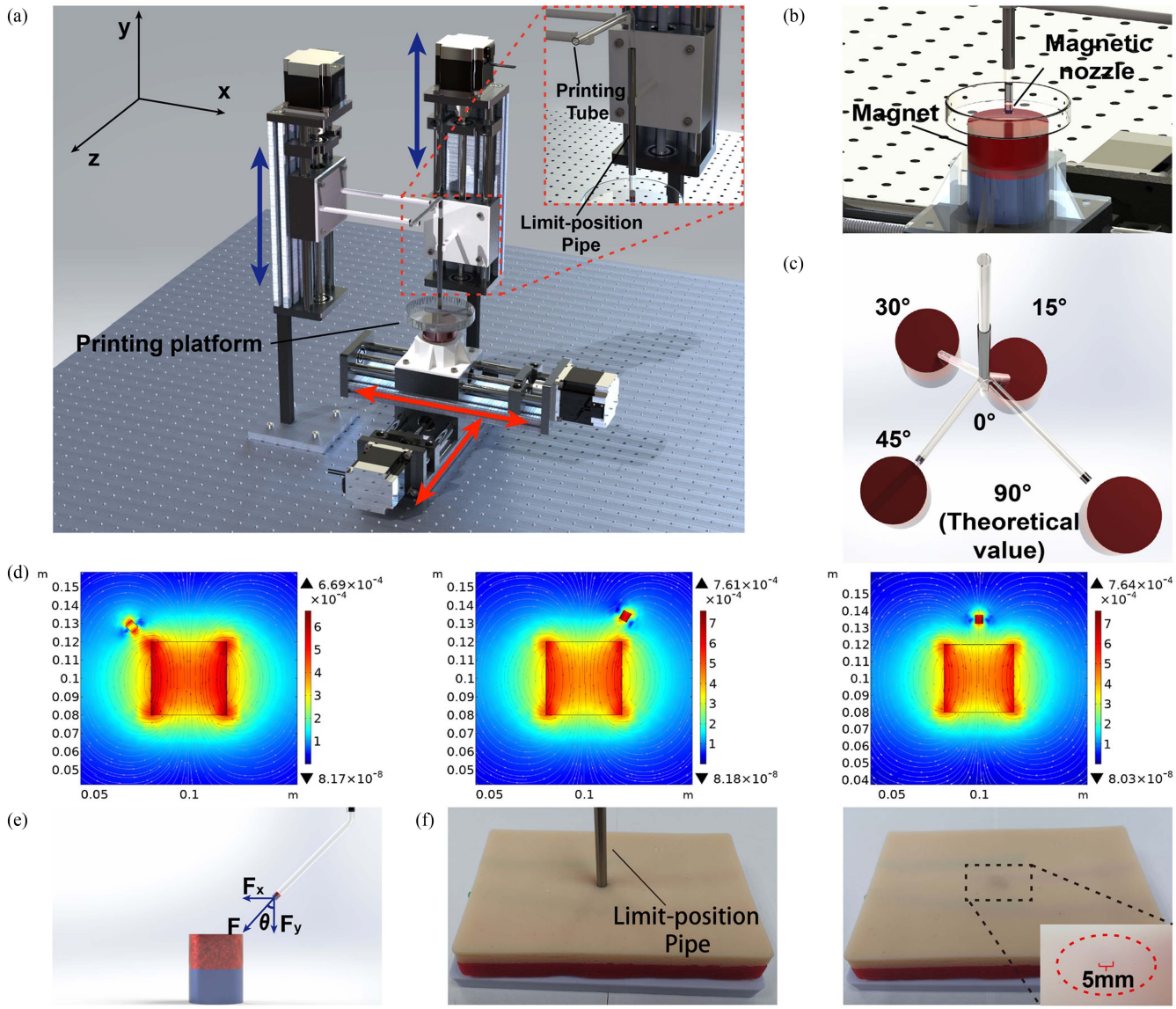

Fig. 2. Overall structure and detail sections of the printing system. (a) Structure diagram of the printing system. Red arrows represent horizontal displacement, and blue arrows represent vertical displacement. (b) Details of the printing platform. (c) The bending angle of flexible pipe and its position relative to the magnet. 90° is only theoretically possible. (d) Simulation results of the magnetic field when the nozzle and guidance magnet are in different positions on the same plane. (e) Force is imposed on the nozzle in the magnetic field of the guidance magnet. F represents the total force, F_x is the radial force, and F_y denotes the axial force. (f) The experiment of the limit-position pipe entering into the skin model with an enlarged view of its incision size. The incision is barely visible to human eyes.

the guidance magnet is located at four positions, where the angles between the tangent line at the bend of the printing tube and the limit-position pipe are denoted. Among these four positions influenced by the printing tube's elasticity, the angle of 90° is a theoretical value when the XZ plane is parallel to the upper surface of the guidance magnet. Fig. 2(d) shows the distribution of magnetic flux density when the angle between the tangent line at the bend of the printing tube and limit-position pipe is 45°, 30°, and 0°, respectively.

The translational displacement of the guidance magnet will alter the magnetic field in space and then drive the printing tube and nozzle to bend, producing a translational displacement. At the same time, the nozzle will undergo an upward displacement in the Y-axis. Therefore, to compensate for the deviation from the Y-axis, the motor connected to the printing tube in the Y-axis can be controlled so that the printing tube can be moved downward by a displacement with a magnitude identical to the nozzle's upward displacement. When printing multilayered structures on non-planar surfaces, the compensation displacement in the Y-axis should be adjusted by considering the surface morphology in different situations. It is essential to keep the nozzle fixed relative to the printing surface to ensure better printing results. By mapping the angle (between the tangent line at the bend of printing tube and limit-position pipe) and the Y-axis displacement of the nozzle to control program, we can adjust the movement of the guidance magnet to precisely produce desired movement of the nozzle. It realizes magnetically driven printing progress in a variety of complex situations.

When the nozzle is located within the effective range of the guidance magnet, the nozzle experiences a force imposed by the

guiding magnet's magnetic field. According to magnetic theory, the standing of the nozzle in a magnetic field can be attributed to the force exerted by the molecular current. In particular, when the nozzle is located in a magnetic field, the internal magnetization current exists, and the surface magnetization current emerges on the nozzle surface. The magnetization electro-fluid density and surface magnetization current's density are derived as:

$$\delta_v = \bigtriangledown \cdot M \tag{1}$$

$$\delta_s = -n \cdot M \tag{2}$$

where M is the dielectric reinforcement strength and n is the surface normal vector of the guidance magnet.

The force imposed on the nozzle by the magnetic field of the guidance magnet is calculated by

$$F = \iiint_v \delta_v \cdot B dv + \oint_s \delta_s \cdot B ds$$

$$F = \iiint_v (\bigtriangledown \cdot M) \cdot B dv + \oint_s (-n \cdot M) \cdot B ds \tag{3}$$

where B is the magnetic induction strength. For each homogeneous medium, we have

$$F = \iiint_v (\bigtriangledown \cdot M) \cdot B dv \tag{4}$$

with

$$M = \frac{\mu_r - 1}{\mu_r \mu_0} B \tag{5}$$

where μ_0 is the vacuum permeability and μ_r is the relative permeability of the magnetic medium.

Then, vector operation gives

$$F = \frac{\mu_r - 1}{2\mu_r \mu_0} \iiint_v \bigtriangledown B^2 dv \tag{6}$$

In view of the vector gradient integration equation:

$$\iiint_v \bigtriangledown \varphi dv = \iint_s \varphi \cdot ds \tag{7}$$

the force on the nozzle in the magnetic field of the guiding magnet is derived below.

$$F = \frac{\mu_r - 1}{2\mu_r \mu_0} \iint_s B^2 \cdot ds \tag{8}$$

C. Hybrid Tube Design

As shown in Fig. 1(c), the conventional magnetically driven printing device imposes practical issues for in vivo and in vitro use, which produces a relative displacement of the printing tube and skin contact during the printing process. The contact part between the printing tube and human skin would be torn apart to a certain extent during the movement of the printing tube. To overcome this issue, we introduce the concept of hybrid tube by adding a limit-position rigid pipe to support the flexible printing tube for moving below the human skin to avoid tears on the skin.

By using the limit-position pipe in the human body, only a tiny incision in the skin model is required. When the in vivo printing operation is completed, the limit-position pipe can be easily removed, leaving only a small incision. As shown in Fig. 2(f), the small incision has the maximum length of approximately 5 mm. It also helps to relieve the pain of patients in practice.

The adopted printing tube in the system is made of silica gel. According to its own characteristics, if the moving part of the printing tube in the printing process is too long, irregular jittering of the printing tube would be caused. After adding the limit-position pipe, the jittering can be avoided by adjusting relative position of the end of limit-position pipe and nozzle. During printing, the motor can regulate the limit-position pipe to move up and down to change the motion range of the nozzle, so that the maximum printing range of the nozzle can be adjusted.

III. Nozzle Optimization

It is observed that the nozzle can shift during the printing operation as the functional ink flows through the printing tube, especially with the nozzle material of NdFeB. NdFeB is a powerful permanent magnet material, whose magnetic energy product is between 27 and 50 MGOe. However, considering that the fracturez toughness K_{1c} of the NdFeB material is only 2.2—5.5 MPa$\cdot$ m$^{\frac{1}{2}}$, we need to optimize the structure at the nozzle to prevent the magnet nozzle from being pushed out of the original position. Here, a fluid stabilizer has been added above the magnetic nozzle to protect the magnetic nozzle (Fig. 3(a)). Fig. 3(b) demonstrates the cutaway of the fluid stabilizer. The fluid stabilizer is made by 3D printing with polylactic acid (PLA). Its interior has been designed to be streamlined. Such design can prevent the heap of functional ink as it enters the nozzle. It also greatly reduces the resistance of the functional ink during feeding process.

Before adding the fluid stabilizer, the functional ink's flow rate changes abruptly at the nozzle inlet. The maximum flow rate at the geometric center is faster (Fig. 3(c)). By adding the fluid stabilizer, the functional ink's flow velocity change is shifted to the stabilizer inlet. The maximum flow velocity zone is longer than the former, and the maximum flow rate has been reduced by 10%. Meanwhile, Fig. 3(e) illustrates the fluid impact stress on the magnetic nozzle without installing a fluid stabilizer. It is found that the stress on the nozzle is particularly pronounced at the entry point, where it comes into contact with the functional ink. By adding a fluid stabilizer, the stress on the nozzle has been significantly reduced as compared to the former (Fig. 3(f)). Hence, the addition of a fluid stabilizer has a significant protective effect on the magnetic nozzle and improves the printing efficiency.

IV. Experimental Testing and Result

In this section, the performance of the developed bioprinting system is tested to demonstrate its printing capability.

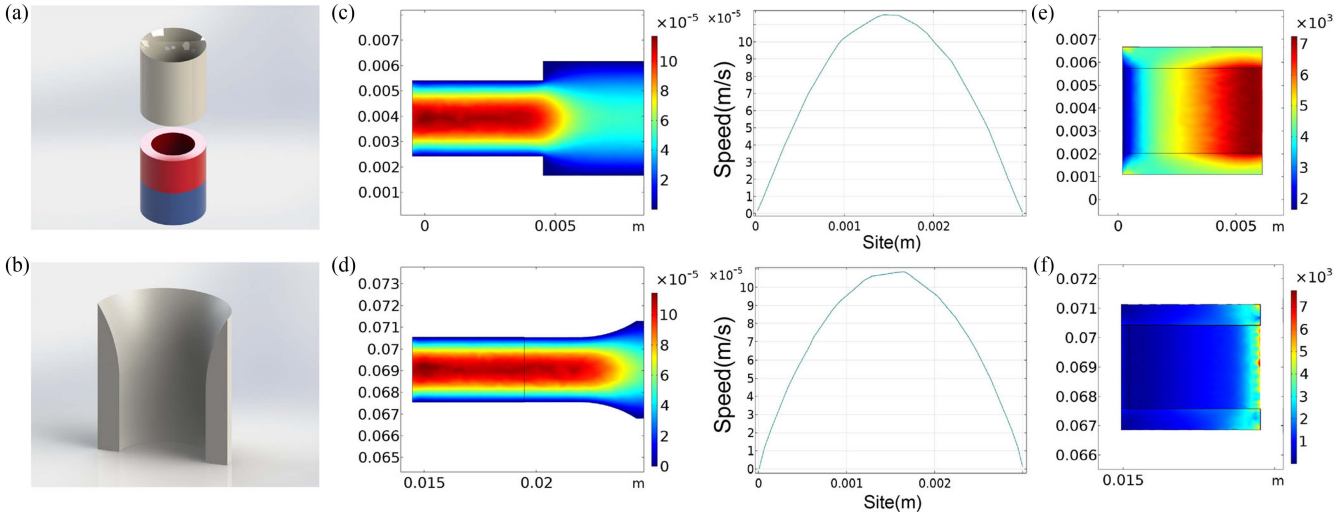

Fig. 3. Nozzle optimization and simulation results. (a) Structure diagram of the optimized nozzle. The bottom half represents the original magnetic nozzle, and the top half is a fluid stabilizer which is added for optimization. (b) Cutaway view of the fluid stabilizer. (c) Functional ink's flow rate distribution in printing tube before optimization and flow rate profile at the nozzle. (d) Functional ink's flow rate distribution in printing tube after optimization and flow rate profile at the nozzle. (e) Stress simulation result of magnetic nozzle profile before optimization. (f) Stress simulation result of magnetic nozzle profile after optimization.

A. Test Result of Relationship Between the Nozzle and Magnetic Field

In the experimental test, we found that due to the distribution and movement of the magnetic field, the nozzle needs to be well controlled by the guidance magnet to achieve accurate printing results. Hence, we analyzed the relationship between the main parameters of the guidance magnet and printing tube to achieve better results. Fig. 4(a) demonstrates the relative distance (t) from the center of guidance magnet to the center of nozzle, the angle (θ) between the tangent line at the bend of flexible printing tube and limit-position rigid pipe, and the straight distance (L) between the nozzle and bottom of the limit-position pipe, i.e., the printing tube's protrusion length.

First, we analyzed the relationship between t and θ under a guidance magnet with the diameter of 30 mm, 40 mm, and 50 mm, respectively. It is found that under different diameters of the guidance magnet, the ratio t/D increases as the angle θ rises (Fig. 4(b)). In addition, as θ keeps larger, the trend of the ratio t/D (with different diameters of guidance magnet) tends to be the same.

Moreover, by selecting the guidance magnet's diameter as 30 mm, we have tested the variation trend of t versus θ when different materials (NdFeB and NiZnFeO) are adopted for the nozzle (Fig. 4(c)). The comparison shows that the variation trend of t is steeper when NdFeB rather than NiZnFeO is adopted as the nozzle material. Comparing the magnetic strength of these two kinds of nozzles, we can conclude that the guidance magnet is more effective in guiding the nozzle which is produced by the material with more powerful magnetic field.

In addition, the maximum effective angle ($\theta_{\max}$) indicates the maximum angle value at which the printing tube could return to its original position with the guidance magnet displacement during the printing process. We compared the maximum effective angle under different protrusion lengths (L) of the printing tube. By fitting the data (Fig. 4(d)), we found that after a short sharp rise in $\theta_{\max}$, the change leveled off near 40° and became constant at 45°. Consequently, the maximum value $\theta_{\max} = 45°$ is selected to ensure the accuracy of the printing process.

B. Results of Printing Experiment

We conducted an experimental study to test the consistency of printing performance during the deflection of flexible tube induced by magnetic force. Fig. 4(e) shows the working principle of printing circles of different radii R_n by the system in case of different deflection angles θ. By selecting five different positions on the circle, we calculated the standard deviation σ of the errors between actual and theoretical radii of the circle. Fig. 4(f) shows the variation tendency of σ versus θ under different L values. The variation tends to be stable when θ is less than 45°, where the deflection of flexible tube has negligible effect on the printing performance. When θ is greater than 45°, the change in σ becomes steeper. Thus, it is reasonable to set the maximum deflection angle of the flexible tube as 45°.

In the literature, quantitative evaluation of printing accuracy in two dimensions has been widely used by many researchers [30]. The evaluation is realized by printing a 2-layer vertical pattern. Then, the actual perimeter L and area A of each hole are measured after printing. By using P_r as a quantitative factor, the printing accuracy (Fig. 4(g)) is defined by the equation: $P_r = \frac{L^2}{16A}$.

Fig. 4(h) depicts the variation trend of P_r versus the printing speed, where the gray area represents acceptable printability region. Fig. 4(i) shows the variation trend of P_r as the distance s between the nozzle and substrate surface increases. By inspecting the two curves, it is evident that optimization of the nozzle can significantly improve the printing performance. We found that without optimization, the filament could not be formed if the printing speed is less than 0.42 ml/min. After optimization, the filament could be formed when the printing speed is greater than 0.36 ml/min. Hence, the optimization has extended the usable range of the printing speed.

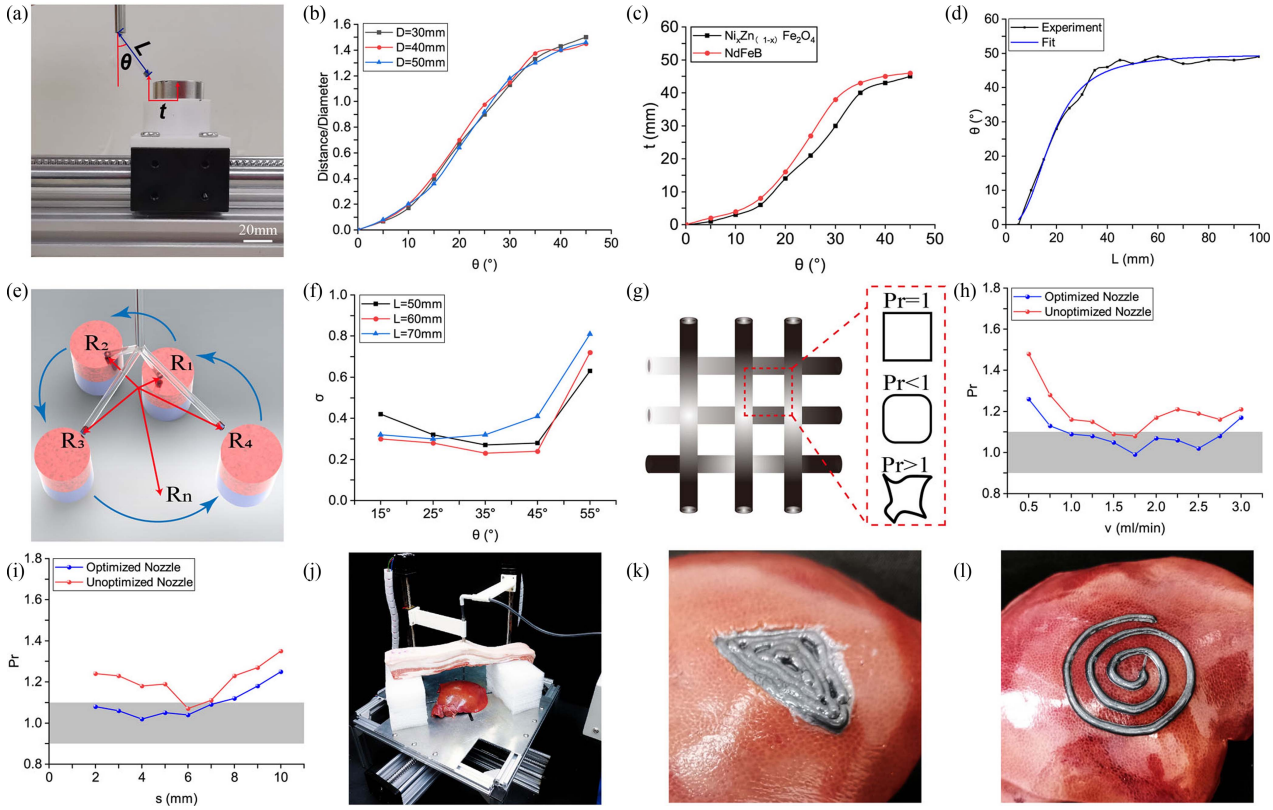

Fig. 4. Experimental results of the printing system. (a) The relative position of the guidance magnet and nozzle. t is the relative distance from the guidance magnet's center to the nozzle's center. θ is the angle between the tangent line at the bend of the printing tube and limit-position rigid pipe. L is the straight distance between the nozzle and the bottom of limit-position pipe, i.e., the printing tube's protrusion length. (b) Relationship of the ratio (t/D) of relative distance between the center of guidance magnet and the center of nozzle to the diameter of the guidance magnet versus the angle θ between the tangent line at the bend of printing tube and limit-position pipe. (c) Relationship of the relative distance (t) from the center of guidance magnet to the center of nozzle versus the angle θ with different materials (NdFeB and NiZnFeO) for the nozzles. (d) Relationship of the straight distance (L) between the nozzle and bottom of the limit-position pipe versus the maximum angle ($\theta_{\max}$) between the tangent line at the bend of printing tube and limit-position pipe. (e) Schematic of printing performance consistency test. (f) The standard deviation of the errors between actual and theoretical printing radii under different θ values. (g) Schematic of printing accuracy test. (h) Variation curve of printing accuracy P_r versus the printing speed. (i) Variation curve of printing accuracy P_r versus distance s between the nozzle and substrate surface. (j) Photo of experimental setup for the printing system. (k) Notch-fill printing test on a pig liver tissue. (l) Pattern printing test on a pig liver tissue.

The developed bioprinting system can print various patterns on both planar and non-planar surfaces in a minimally invasive manner. We conducted several groups of experiments by using Ecoflex and toner composite as the functional ink. First, we used pig liver tissue to evaluate the printing performance under the pig skin (Fig. 4(j)). We cut a triangular notch in the pig liver tissue, and then filled the notch by printing (Fig. 4(k)). In addition, we have conducted the printing of circular patterns on the surface of pig liver tissue (Fig. 4(l)). The experimental results demonstrate the effectiveness of the proposed system for printing on biological tissue surface.

Then, we tested two groups of single-layer printing on flat surfaces by printing the letter "G" (Fig. 5(a)) and "UM" (Fig. 5(b)). These two printing patterns show good consistency with the original letters, which verifies the reliability of our printing system. Second, we tested two groups of multi-layer printing on flat surfaces by printing the letter "X" with five layers (Fig. 5(c)) and "S" (Fig. 5(d)) with four layers.

Due to viscoelastic nature of the material, the functional ink usually has a phenomenon of die-swelling when it starts to be extruded. As a result, a printed fiber of diameter αd is obtained, where d is the inner diameter of the printing nozzle and α is the swelling ratio. The resolution of the printed fibers depends on four main parameters: the speed of movement of the nozzle, the input pressure, the inner diameter of the nozzle, and the viscosity of the ink. A faster moving speed tends to stretch the printed fiber, leading to a smaller αd. While increasing the input speed, the size of the inner diameter and the viscosity will increase αd. Note that the nozzle speed should be well controlled to ensure that there is no accumulation or discontinuity in the continuously printed fibres [31], [32].

C. Further Discussion

The performances of typical bioprinting systems are tabulated in Table I. Compared to other works, the proposed concept of a hybrid tube (integrating a limit-position rigid pipe and a flexible printing tube) allows for minimally invasive abdominal or thoracic surgery operations.

The proposed minimally invasive bioprinting system is still in its infancy and has limitations regarding print speed, resolution, and complexity of the printed patterns. More magnetic domain tuning and printing tube curvature adjustment are required to handle intricate 3D designs and constrained biological contexts.

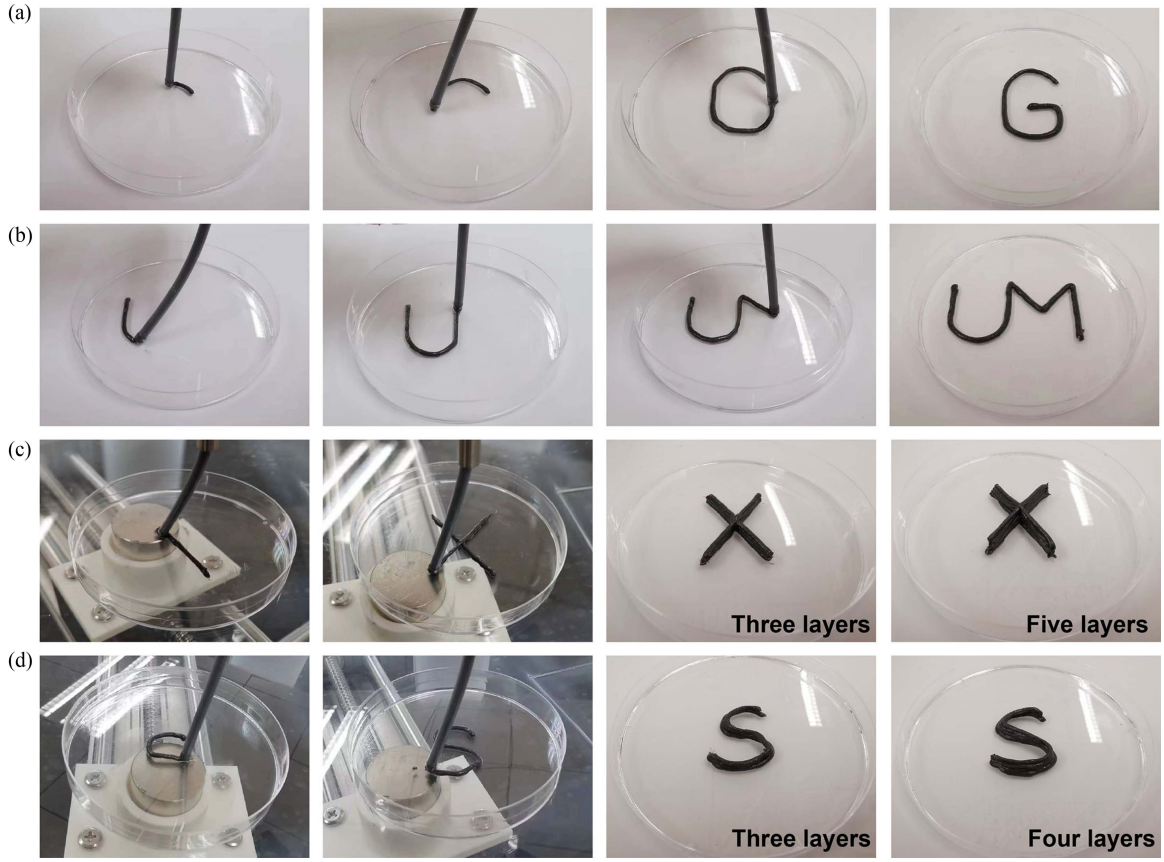

Fig. 5. Experimental results of printing process for the bioprinting system. (a) Demonstration of printing the letter G. (b) Demonstration of printing the letters U and M. (c) Demonstration of five-layered printing of the letter X. (d) Demonstration of four-layered printing of the letter S.

TABLE I
PERFORMANCE COMPARISON OF TYPICAL BIOPRINTING SYSTEMS

References	Actuation Method	Printing Position	Incision Size	Max. Depth	Max. Printing Radius
[1]	Mechanical	Thorax/Abdomen	>10 mm	100 mm	N/A
[14]	Mechanical	Stomach	>30 mm	60 mm	15 mm
[16]	Magnetic	Thorax/Abdomen	>4 mm	N/A	20 mm
[20]	Mechanical	Bones	5 mm*2	1-10 mm	N/A
This Work	Magnetic	Thorax/Abdomen	3-5 mm	120 mm	32 mm

In addition, more adaptable magnetic fields may be created, for instance, by defining the requirements for guiding magnets or by combining guiding magnets to create a composite field. In the future, a more user-friendly control scheme will be designed to facilitate the operator or doctor to complete the printing work. The present work is focused on the printing method and hybrid tube design. In future work, we will conduct more printing experiments in thorax or abdomen cavity to further improve the system.

Furthermore, the advances in functional materials, which are bioprintable, will enable the system to print more complex 3D patterns/structures onto curved or wet surfaces. Due to the constrained anatomical context, minimally invasive bioprinting may not be suitable for such curing conditions. Bioinks can cure through liquid evaporation, gelation, and temperature- or solvent-induced phase shifts. The printed structure may collapse before it cures, especially when printing complicated 3D buildings. Consequently, it is crucial to speed up the curing process of injectable inks and employ biodegradable support molds in the future.

V. CONCLUSION

In this work, we introduced a bioprinting system dedicated to minimally invasive surgery. The system is implemented by combining magnetic actuation with 3D printing technology. The interaction of the nozzle in a magnetic field environment is explained by performing a computational magnetic field simulation study. The simulation results reveal how the guide magnet affects the gravitational force acting on the nozzle while its tangent moves in the left, center, or right direction. By simulating the fluid-solid coupling of the nozzle and optimizing the design parameters, we have improved the system's stability in printing. Moreover, the relationship between the guidance magnets and

the nozzle was analyzed, and the results indicated that the nozzle material, nozzle extension length, and diameter of the guiding magnets govern the displacement of the nozzle. We also analyze whether the printing performance changes when the printing tube is deflected and the effect of printing speed and nozzle height on printing accuracy. Finally, the feasibility of the proposed system was revealed by conducting an experimental study through pig skin on pig liver tissue with different patterns printed in single and multiple layers. The results reported in this work demonstrate how minimally invasive printing collectively paves the way for future application of minimally invasive bioprinting in a remote, interoperable, and more secure manner.

REFERENCES

[1] A. Simeunović, K. Wolf, K. Tierling, and D. J. Hoelzle, "A surgical robot for intracorporeal additive manufacturing of tissue engineering constructs," *IEEE Robot. Automat. Lett.*, vol. 7, no. 3, pp. 7495–7502, Jul. 2022.

[2] S. V. Murphy and A. Atala, "3D bioprinting of tissues and organs," *Nature Biotechnol.*, vol. 32, no. 8, pp. 773–785, 2014.

[3] Y. S. Zhang et al., "3D extrusion bioprinting," *Nature Rev. Methods Primers*, vol. 1, no. 1, pp. 1–20, 2021.

[4] C. Mandrycky, Z. Wang, K. Kim, and D.-H. Kim, "3D bioprinting for engineering complex tissues," *Biotechnol. Adv.*, vol. 34, no. 4, pp. 422–434, 2016.

[5] Y. S. Zhang et al., "3D bioprinting for tissue and organ fabrication," *Ann. Biomed. Eng.*, vol. 45, no. 1, pp. 148–163, 2017.

[6] G. Singh, S. Mehta, A. Saini, and B. Pabla, "Advances in additive manufacturing techniques for bioprinting," *ECS Trans.*, vol. 107, no. 1, 2022, Art. no. 6273.

[7] Y. Zhang et al., "Recent advances in cardiac patches: Materials, preparations, and properties," *ACS Biomaterials Sci. Eng.*, vol. 8, no. 9, pp. 3659–3675, 2022.

[8] A. C. Daly, M. E. Prendergast, A. J. Hughes, and J. A. Burdick, "Bioprinting for the biologist," *Cell*, vol. 184, no. 1, pp. 18–32, 2021.

[9] W. Sun et al., "The bioprinting roadmap," *Biofabrication*, vol. 12, no. 2, 2020, Art. no. 022002.

[10] I. T. Ozbolat, W. Peng, and V. Ozbolat, "Application areas of 3D bioprinting," *Drug Discov. Today*, vol. 21, no. 8, pp. 1257–1271, 2016.

[11] Z. Zhu et al., "3D printed functional and biological materials on moving freeform surfaces," *Adv. Mater.*, vol. 30, no. 23, 2018, Art. no. 1707495.

[12] N. Hakimi et al., "Handheld skin printer: In situ formation of planar biomaterials and tissues," *Lab Chip*, vol. 18, no. 10, pp. 1440–1451, 2018.

[13] N. Ashammakhi et al., "In situ three-dimensional printing for reparative and regenerative therapy," *Biomed. Microdevices*, vol. 21, no. 2, pp. 1–6, 2019.

[14] W. Zhao and T. Xu, "Preliminary engineering for in situ in vivo bioprinting: A novel micro bioprinting platform for in situ in vivo bioprinting at a gastric wound site," *Biofabrication*, vol. 12, no. 4, 2020, Art. no. 045020.

[15] M. Price et al., "Generative design for additive manufacturing using a biological development analogy," *J. Comput. Des. Eng.*, vol. 9, no. 2, pp. 463–479, 2022.

[16] C. Zhou et al., "Ferromagnetic soft catheter robots for minimally invasive bioprinting," *Nature Commun.*, vol. 12, no. 1, pp. 1–12, 2021.

[17] L. Y. Daikuara et al., "3D bioprinting constructs to facilitate skin regeneration," *Adv. Funct. Mater.*, vol. 32, no. 3, 2022, Art. no. 2105080.

[18] M. Hospodiuk, M. Dey, D. Sosnoski, and I. T. Ozbolat, "The bioink: A comprehensive review on bioprintable materials," *Biotechnol. Adv.*, vol. 35, no. 2, pp. 217–239, 2017.

[19] D. Chimene, R. Kaunas, and A. K. Gaharwar, "Hydrogel bioink reinforcement for additive manufacturing: A focused review of emerging strategies," *Adv. Mater.*, vol. 32, no. 1, 2020, Art. no. 1902026.

[20] M. Xie et al., "In situ 3D bioprinting with bioconcrete bioink," *Nature Commun.*, vol. 13, no. 1, pp. 1–12, 2022.

[21] M. K. Kim, W. Jeong, S. M. Lee, J. B. Kim, S. Jin, and H.-W. Kang, "Decellularized extracellular matrix-based bio-ink with enhanced 3D printability and mechanical properties," *Biofabrication*, vol. 12, no. 2, 2020, Art. no. 025003.

[22] K. Markstedt, A. Mantas, I. Tournier, H. Martínez Ávila, D. Hagg, and P. Gatenholm, "3D bioprinting human chondrocytes with nanocellulose–alginate bioink for cartilage tissue engineering applications," *Biomacromolecules*, vol. 16, no. 5, pp. 1489–1496, 2015.

[23] K. Guo et al., "Collagen-based thiol–norbornene photoclick bio-ink with excellent bioactivity and printability," *ACS Appl. Mater. Interfaces*, vol. 13, no. 6, pp. 7037–7050, 2021.

[24] J. Chakraborty, X. Mu, A. Pramanick, D. L. Kaplan, and S. Ghosh, "Recent advances in bioprinting using silk protein-based bioinks," *Biomaterials*, vol. 287, 2022, Art. no. 121672.

[25] Z. U. Arif, M. Y. Khalid, A. Zolfagharian, and M. Bodaghi, "4D bioprinting of smart polymers for biomedical applications: Recent progress, challenges, and future perspectives," *Reactive Funct. Polymers*, vol. 179, 2022, Art. no. 105374.

[26] Q. Wang et al., "Untethered small-scale machines for microrobotic manipulation: From individual and multiple to collective machines," *ACS Nano*, vol. 17, no. 14, pp. 13081–13109, 2023.

[27] P. D. Costa, D. C. Costa, T. R. Correia, V. M. Gaspar, and J. F. Mano, "Natural origin biomaterials for 4D bioprinting tissue-like constructs," *Adv. Mater. Technol.*, vol. 6, no. 10, 2021, Art. no. 2100168.

[28] P. J. Díaz-Payno et al., "Swelling-dependent shape-based transformation of a human mesenchymal stromal cells-laden 4D bioprinted construct for cartilage tissue engineering," *Adv. Healthcare Mater.*, vol. 12, no. 2, 2022, Art. no. 2201891.

[29] Z. Wu, Y. Zhang, N. Ai, H. Chen, W. Ge, and Q. Xu, "Magnetic mobile microrobots for upstream and downstream navigation in biofluids with variable flow rate," *Adv. Intell. Syst.*, vol. 4, no. 7, 2022, Art. no. 2100266.

[30] L. Ouyang, R. Yao, Y. Zhao, and W. Sun, "Effect of bioink properties on printability and cell viability for 3D bioplotting of embryonic stem cells," *Biofabrication*, vol. 8, no. 3, 2016, Art. no. 035020.

[31] R. G. Larson and P. S. Desai, "Modeling the rheology of polymer melts and solutions," *Annu. Rev. Fluid Mechanics*, vol. 47, no. 1, pp. 47–65, 2015.

[32] H. Yuk and X. Zhao, "A new 3D printing strategy by harnessing deformation, instability, and fracture of viscoelastic inks," *Adv. Mater.*, vol. 30, no. 6, 2018, Art. no. 1704028.